Chapter 1

Numerical Analysis of Broadband Dipole-Loop Graphene Antenna for Applications in Terahertz Communications

Costa Karlo Queiroz da,
Sousa Gleida Tayanna Conde de,
Gabriel Silva Pinto and Andrey Viana Pires

Additional information is available at the end of the chapter

http://dx.doi.org/10.5772/intechopen.74936

Abstract

Graphene possesses good properties as unusually high electron mobility, atomic layer thickness, and unique mechanical flexibility, which made it one promising material in the design of terahertz antennas. In this book chapter, we present a numerical analysis of a broadband dipole-loop graphene antenna for application in terahertz communications. The bidimensional method of moments (MoM-2D), with equivalent surface impedance of graphene, is used for numerical analysis. First, we review the principal characteristics of the conventional rectangular graphene dipole. Then, we consider the broadband graphene antenna, composed by one rectangular dipole placed near and parallel to a circular-loop graphene element, where only the dipole is feed. In this analysis, we investigated the effects of the geometrical parameters and the chemical potential, of the graphene material, on the overall characteristics of the compound antenna. Some results are compared with simulations performed with software based on finite element method. The results show that this simple compound graphene antenna can be used for broadband communications in the terahertz band.

Keywords: graphene antenna, broadband dipole-loop antenna, terahertz radiation, method of moment (MoM), graphene surface impedance

1. Introduction

Over the last few years, wireless data traffic has drastically increased due to a change in the way today's society creates, shares, and consumes information. This change has been accompanied

by an increasing demand for a much higher speed wireless communication anywhere, anytime. Advanced physical layer solutions and, more importantly, new spectral bands will be required to support these extremely high data rates [1].

In this context, terahertz (THz) band communication [2–8] is envisioned as a key wireless technology to satisfy this demand; it is an alternative to spectrum demand and capacity limitations of current wireless systems, allowing multitude of applications. The THz band is the spectral band that spans the frequencies between 0.1 and 10 THz. While the frequency regions immediately below and above this band (the microwaves and the far infrared, respectively) have been extensively investigated, this is still one of the least-explored frequency bands for communication [1].

Therefore, there is a need to develop new transceiver antennas that are able to operate in THz frequencies in a very large operating bandwidth. Different technologies are actually in development in literature. In this chapter, we focus on graphene technology for the design of broadband terahertz antennas.

Graphene is a monolayer of carbon atoms arranged in a two-dimensional hexagonal honeycomb lattice [9]. The exceptional properties of graphene like unusually high electron mobility, atomic layer thickness, and possibility of miniaturizing antennas based on this material and many other properties made it one promising material in many areas ranging from solar cells [10] to ultra-high-speed transistors [11].

Significant benefits can be obtained for graphene antennas in telecommunications applications such as monolithic integration with nanoelectronic graphene radio frequency (RF), efficient dynamic adjustment through chemical potential, relatively low loss in the band of terahertz (THz), and the possibility of miniaturization of antennas due to common plasmon effect in metamaterials [12, 13]. On the other side, there are few alternatives and works in literature about broadband graphene antennas [14, 15].

In this chapter, a theoretical analysis was made in a broadband graphene antenna composed by a rectangular dipole and a circular loop. The analysis is made using the two-dimensional method of moments (MoM 2D) with surface impedance [15, 16]. It was calculated by input impedance, reflection coefficient, and bandwidth from antennas with different geometrical parameters and values of chemical potential in the range of 0.5–2 THz. Some results were obtained by finite element method (FEM) with the Comsol software for comparison [17].

2. Antenna geometry

Figure 1 shows the geometry of the proposed broadband graphene antenna. This antenna is composed of two elements: a rectangular planar dipole with dimensions L and W, with same values used in [13] for comparison, and a circular passive ring (or circular loop) with inner radius R1 and outer radius R2. The environment in which the elements are inserted has a relative permittivity $\varepsilon_r = 2.4$, which is the average of air and substrate permittivity used in [13], where in this reference, the substrate is in $z < 0$. In other words, here we use an equivalent effective permittivity for the whole medium, which is considered homogeneous with no substrate.

http://dx.doi.org/10.5772/intechopen.74936

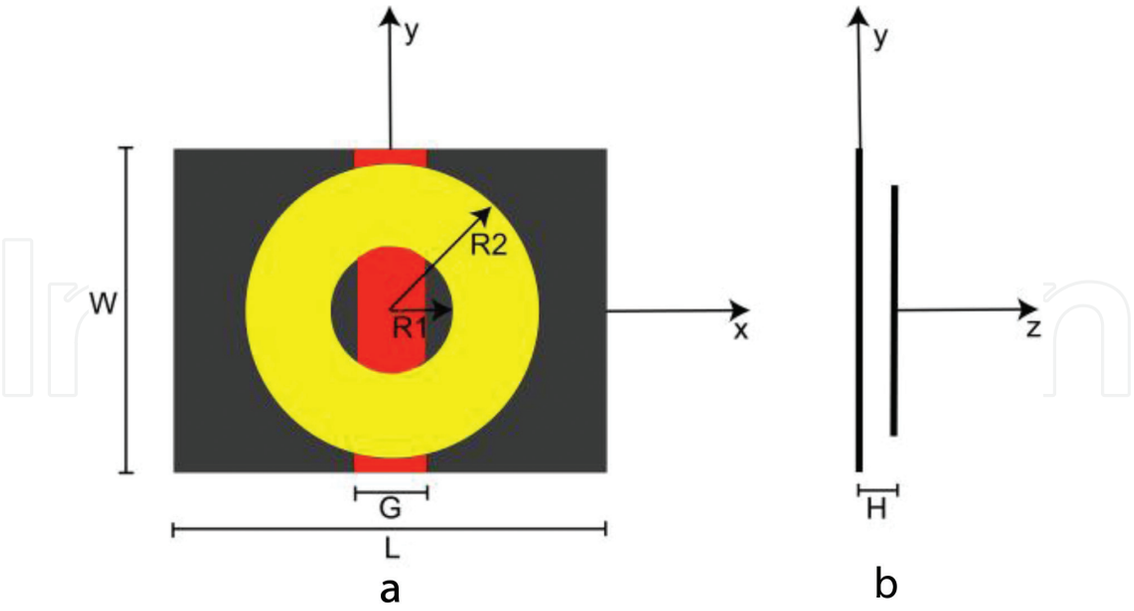

Figure 1. Geometry of the rectangular planar dipole graphene coupled to a circular-loop antenna of the same material: (a) top view and (b) side view.

The two elements are separated by a height H, as shown in **Figure 1**. In the analysis, the geometry of antennas was maintained fixed, that is, the dipole's dimensions and the values of ring's radii (R1 and R2) and height (H) between antennas were fixed, and the chemical potential of graphene circular loop was changed to obtain a broadband operation.

The size of the dipole graphene has only one planar dimension (e.g., W and L) because the graphene thickness is considered very small. This antenna is fed by an equivalent ideal voltage source called photomixer [13] with width W and gap length G in the middle of the dipole shown in **Figure 1**. In MoM, we call it voltage source and, in FEM, we used a lumped port [17].

3. Theoretical development

In this section, the model used for the surface conductivity of graphene, a summary of the MoM-2D model used in the analysis, and details of the Comsol model are presented.

3.1. Graphene surface conductivity

The experimental results show that edge effects on the graphene conductivity can be disregarded in the micrometer scale [15]. Therefore, one can use the electrical conductivity model developed for infinite graphene sheet. In this chapter, we use the Drude model for graphene surface conductivity in the range of 0.5–2 THz

$$\sigma(\omega) = \frac{2e^2 k_B T}{\pi h^2} \ln\left[2\cosh\left(\frac{\mu_C}{2k_B T}\right)\right] \frac{-j}{\omega - j\tau^{-1}} \tag{1}$$

where $\tau = 10^{-12}$ s is the relaxation time, T is the temperature, and μ_C is the chemical potential, which is a function, for example, of a DC voltage applied in graphene sheet [18]. **Figure 2** shows examples of σ for different values of chemical potential with $T = 300$ K.

3.2. Method of moment model

The boundary condition on the antenna surface produces the following integral equation of electric field in frequency domain with temporal dependence $\exp(j\omega t)$:

$$\left[\left(\bar{E}_S + \bar{E}_i\right) \cdot \bar{a}_t\right] \bar{a}_t = Z_S \bar{J} \tag{2}$$

where $\bar{E}_S$ (V/m) is the scattering field from the antenna, $\bar{E}_i$(V/m) is the incident electric field from the voltage source, $\bar{a}_t$ is a unitary vector tangential to the antenna's surface, $\bar{J}$(A/m) is the surface current density of the antenna, and $Z_S = 1/\sigma$ is the surface impedance of graphene. The scattered field is

$$\bar{E}_S = -j\omega\mu_0 \iint_S \bar{J} \frac{e^{-jkR}}{4\pi R} ds' + \nabla\left[\frac{1}{j\omega\varepsilon_0} \iint_S \nabla \cdot \bar{J} \frac{e^{-jkR}}{4\pi R} dS'\right] \tag{3}$$

where j is the imaginary unit, $k = \omega(\mu_0\, \varepsilon_r\, \varepsilon_0)^{1/2}$, ω is the angular frequency (rad/s), μ_0 and ε_0 are the magnetic permeability and electrical permittivity, respectively, in free space, $\varepsilon_r = 2.4$ in the present analysis, and R is the distance between source points and observation points, both on the antenna surface S.

The numerical solution of Eq. (2) by MoM consists in to approximate the surface current on the antenna by a linear combination in a given set of basis function and performs the conventional test procedure with a given set of test function [16]. With this approximation, we transform the integral Eq. (2) in an algebraic linear system which is numerically solved.

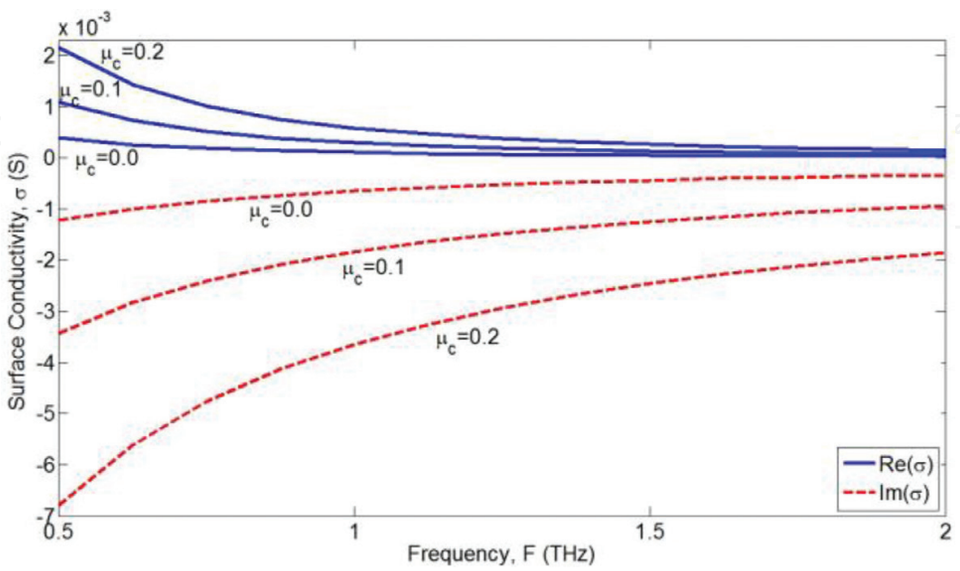

Figure 2. Surface conductivity of graphene versus frequency for different values of μ_C, with $T = 300$ K.

http://dx.doi.org/10.5772/intechopen.74936

3.3. Finite element method model

The Comsol software [17], which is based on the finite element method, was used to simulate examples of graphene antennas to compare our MoM model. The graphene sheet is modeled by an equivalent volumetric electrical conductivity, where it is defined by the surface conductivity (1) divided by the graphene thickness, which was considered finite in the Comsol model $\sigma_V(\omega) = \sigma(\omega)/\Delta$, where Δ is the thickness of the antenna. The domain used is a spherical volume with $\varepsilon_r = 2.4$, where a perfect matched layer (PML) is placed in the outer boundary to absorb the radiated waves. In this model, the dipole is excited by a voltage source with a lumped port element.

4. Numerical results

In this section, we first present the results of two examples of conventional graphene dipole with different sizes. The principal characteristics of this antenna are reviewed. The results are obtained by MoM and FEM models and compared with data of literature [13]. After that, we present the results for the broadband graphene dipole loop. In this case, we analyze the dependence of the radiation and broadband properties of this antenna as a function of the geometry and chemical potential of the loop.

4.1. Conventional graphene dipole

For comparison of our models, this section presents the analysis of the two graphene antennas of the study [13]. The parameters of these antennas are presented in **Table 1**, where we named them Antennas 1 and 2. These two antennas were simulated by MoM and Comsol. The discretization details used in these models are shown in **Figure 3**, where **Figure 3a** and **b** show the meshes used in the MoM method and **Figure 3c** and **d** show the meshes used in the FEM. Note that the meshes in MoM method are only in the surface's antennas, while in the FEM, the meshes are also in a spherical volume around the antennas. This is why the MoM method presents small number of unknowns than the FEM, and consequently, the MoM method requires a smaller computational cost than the FEM.

The input impedance obtained for both antennas is presented in **Figure 4** and the results of input resistance R_{in} and input reactance X_{in} between MoM, simulation Comsol and data from [12] are compared. In general, a good agreement of the results is observed in these figures; the little differences are due to the differences in models and discretizations. The antennas present dipolar resonances similar to conventional RF-microwave antennas, where the fundamental

Antenna	μ_c	L	W
1	0.13 eV	17 μm	10 μm
2	0.25 eV	23 μm	20 μm

Table 1. Parameters of conventional graphene dipole antennas.

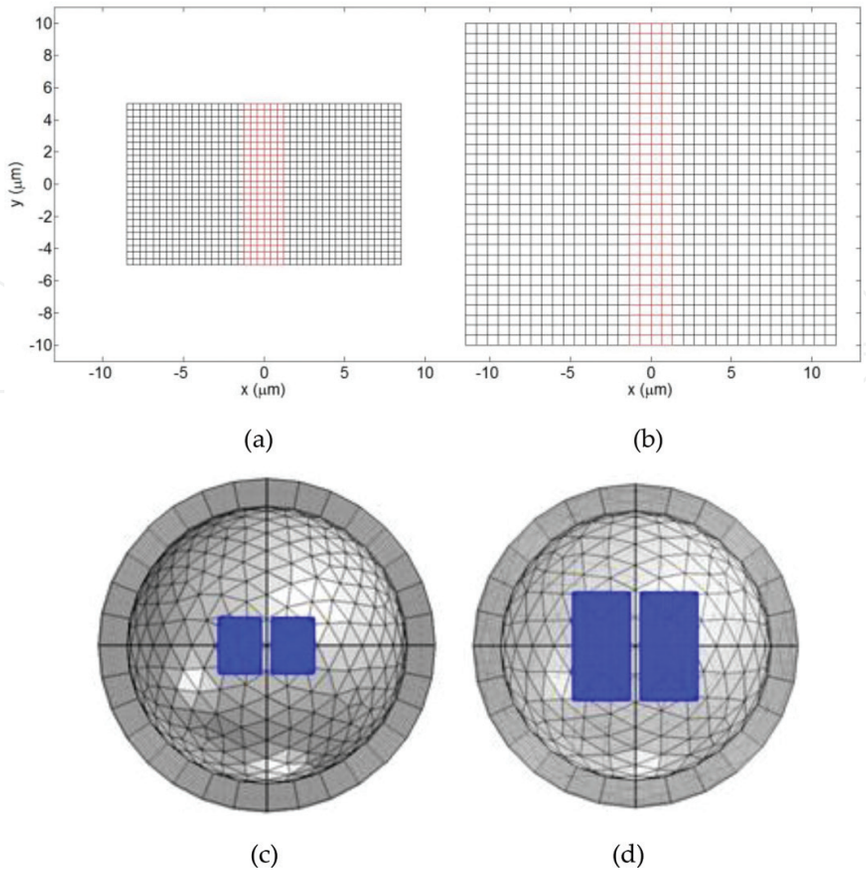

Figure 3. Discretization mesh of graphene antenna used in simulations. (a) Antenna 1—MoM model. (b) Antenna 2—MoM model. (c) Antenna 1—Comsol model. (d) Antenna 2—Comsol model.

resonance is dipolar $\lambda/2$ with lower R_{in} and the second resonance is λ with higher R_{in}. The values of these resonant frequencies are presented in **Table 2**. Antenna 1 possesses a smaller length L than Antenna 2 but the resonances of Antenna 2 are higher than those of Antenna 1; this occur because the chemical potential of Antenna 2 is higher than that of Antenna 1 and this parameter shifts the input impedance to higher frequencies.

Figure 5 shows the reflection coefficient of Antennas 1, when this antenna is matched with a transmission line with characteristic impedance of $Z_c = 100\ \Omega$. In this case, the fractional bandwidth is $B = 11.44\%$, for a reference reflection level of −10 dB. For Antenna 2, this fractional bandwidth is $B = 8.88\%$. These results show that conventional graphene dipoles possess a smaller bandwidth. The next sections present the analysis of broadband graphene dipoles with bandwidths higher than those presented in this section.

4.2. Graphene dipole loop

In this section, we present the numerical results for the broadband graphene dipole-loop antennas of **Figure 1**. First, we make a parametric analysis of geometry and then the effect of chemical potential of loop on the bandwidth and radiation characteristics. The results presented are input impedance, reflections coefficient, bandwidth, and radiation diagram.

http://dx.doi.org/10.5772/intechopen.74936

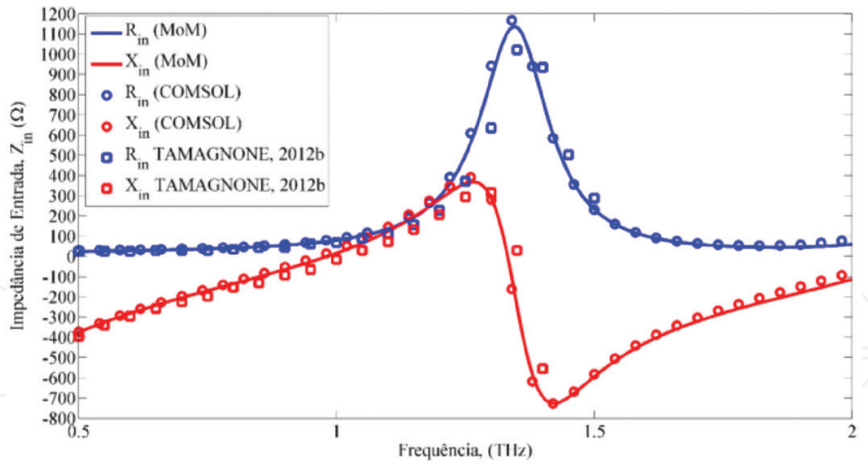

(a)

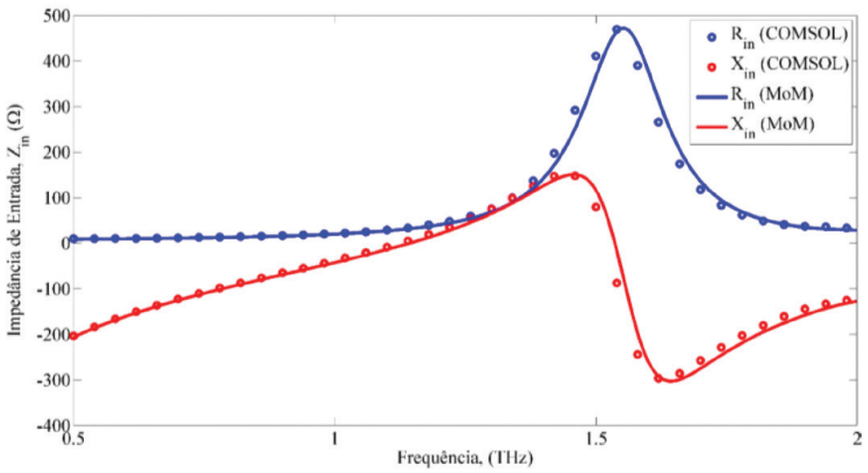

(b)

Figure 4. Input impedance: (a) Antenna 1 and (b) Antenna 2.

	First resonance	Second resonance
MoM	F1 = 0.89 THz	F2 = 1.34 THz
Comsol	F1 = 0.97 THz	F2 = 1.33 THz
Tamagnone [13]	F1 = 1.02 THz	F2 = 1.35 THz

Table 2. Resonant frequencies of Antennas 1 and 2 calculated by different methods.

4.2.1. Parametric analysis with geometry

A parametric analysis of graphene dipole loop of **Figure 1** is presented in this section. We investigate the variation of the characteristics of antenna as a function of the loop's geometry element. In all the analysis, we fixed the size and chemical potential of the dipole with those values of Antennas 1 presented in **Table 1**. In addition, we varied the following parameters of loop element: inner radius R1, outer radius R2, and distance H.

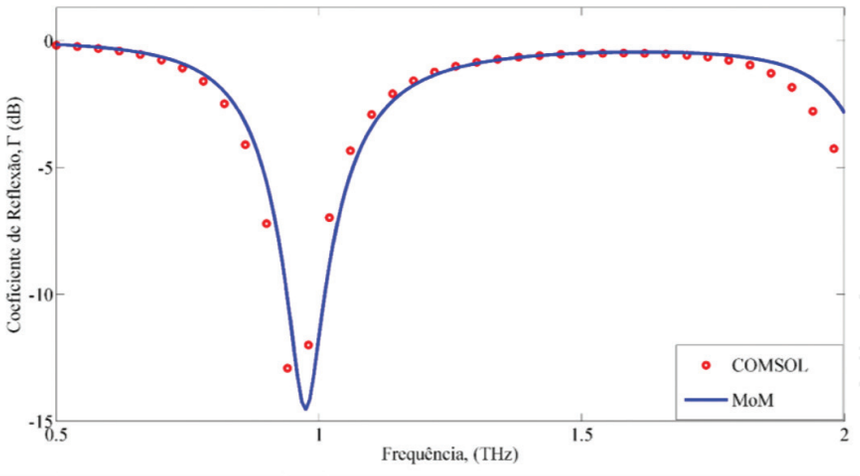

Figure 5. Reflection coefficient of Antenna 1 matched with an impedance feed of Z_c = 100 Ω.

The values of H are varied from 1 to 5 μm. The outer radius R2 presents eight values from 3 to 10 mm, and the inner radius R1 with three fractions of R2, that is, R1 = 0.4 × R2, R1 = 0.6 × R2, and R1 = 0.8 × R2. A total of 120 simulations were done with the MoM code developed. For both elements (dipole and loop), we fixed the potential of μ_C = 0.13 eV (**Table 1**). **Figure 6** shows some examples of graphene dipole loop analyzed with different loop's size and the correspondent mesh used in the MoM model.

For each simulation, we plot the input impedance Z_{in} of the antenna. First, we noted that for higher values of H and R1, the electromagnetic coupling between the dipole and the loop element is smaller. Therefore, the parameters where we obtained best coupling and matching bandwidth are H = 1 mm and R1 = 0.4 × R2. The geometries for some of these cases are presented in **Figure 5d–f**. **Figure 7** shows the input impedances for these cases R2 equal to 3, 4, 5, and 6 μm, and **Figure 8** the Z_{in} for the cases 7, 8, 9, and 10 μm.

In these figures, we can see the effect of the loop and the dipole in the total input impedance. For example, for the case of R2 = 9 mm in **Figure 9**, the resonances of the loop and the dipole are approximately in 0.75 and 1.0 THz, respectively. Also, the loop resonance is shifted to lower frequencies for higher values of R2, and the dipole resonance remains approximately constant. This happens because we are varying only the size of the loop in these simulations, and this size modifies the loop's resonance more strongly.

This behavior of multi-resonance is common for antennas with multiresonant elements coupled electromagnetically, which is the case of the dipole-loop antenna. This analysis of **Figures 7** and **8** shows that we can control the total input impedance so that it presents a broadband characteristic. For this purpose, we choose the loop's size in such a way as to couple the loop and the dipole resonance near to each other to obtain a broader resonance.

To observe this statement, we plot the reflection coefficient of these antennas when they are connected to a transmission line impedance characteristic of Z_c in **Figure 9**. This parameter is calculated by $\Gamma = |(Z_{in}-Z_c)/(Z_{in} + Z_c)|$. A wider bandwidth was obtained when we choose Z_c = 80 Ω for the cases R2 = 3, 4, 5 and 6 μm, and Z_c = 150 Ω for the cases R2 = 7, 8, 9 and 10 μm.

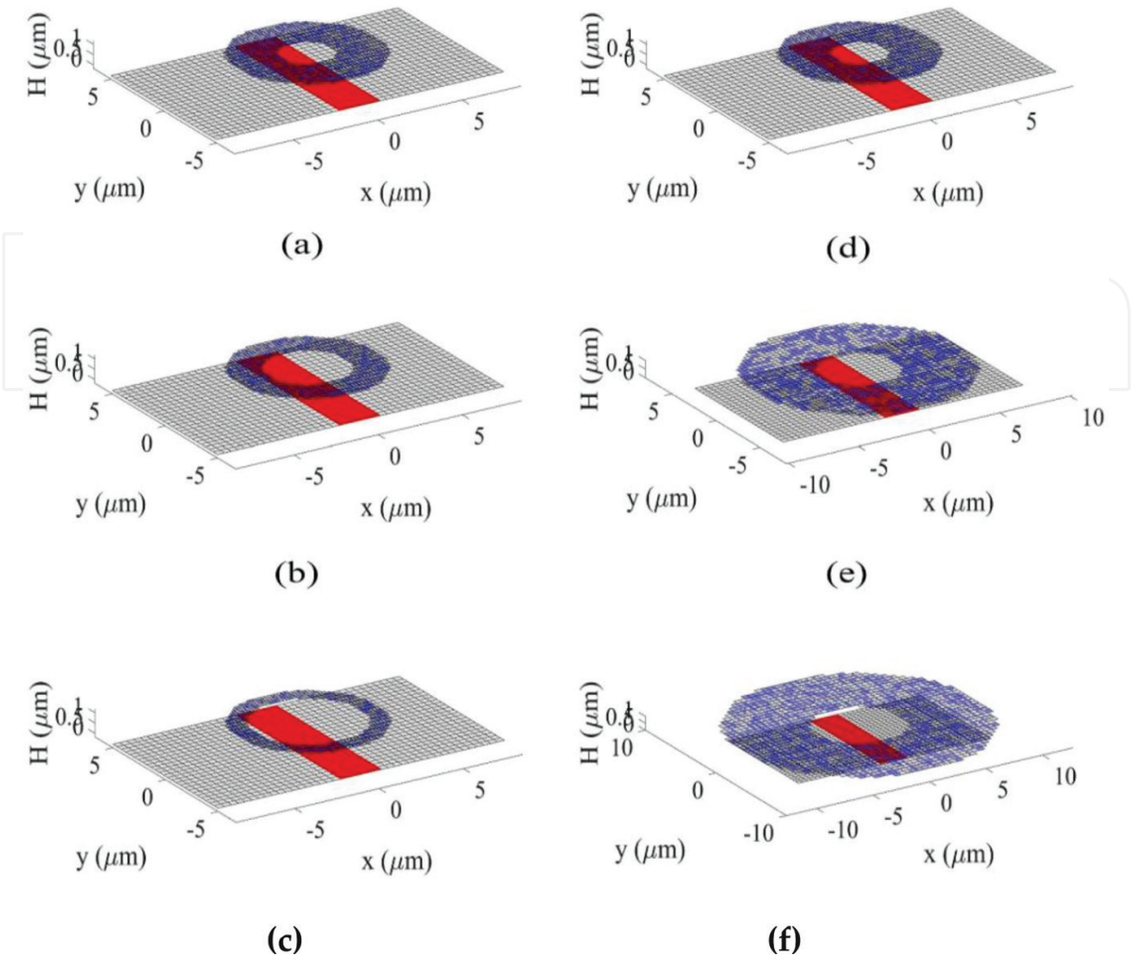

Figure 6. Geometry and mesh of some analyzed examples of graphene dipole-loop antenna with different values of inner radius R1: (a) R1 = 0.4 × R2, (b) R1 = 0.6 × R2, and (c) R1 = 0.8 × R2, and with different values of outer radius R2, where R1 = 0.4 × R2: (d) R2 = 4 μm, (e) R2 = 7 μm, and (f) R2 = 10 μm.

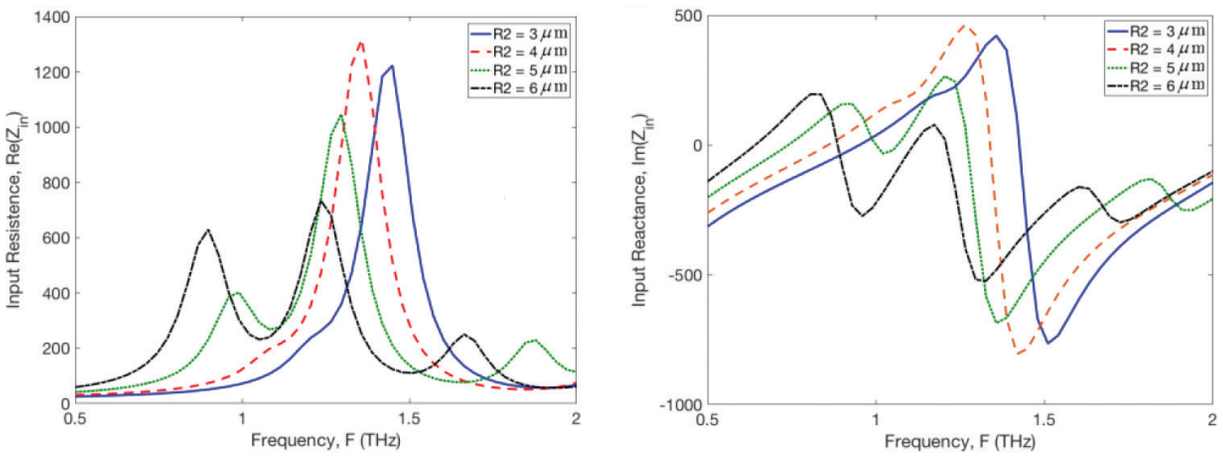

Figure 7. Input impedance for antennas with H = 1 μm, where R1 = 0.4 × R2, R2 = 3, 4, 5, and 6 μm: (a) input resistance ($Re(Z_{in})$) and (b) input reactance ($Im(Z_{in})$).

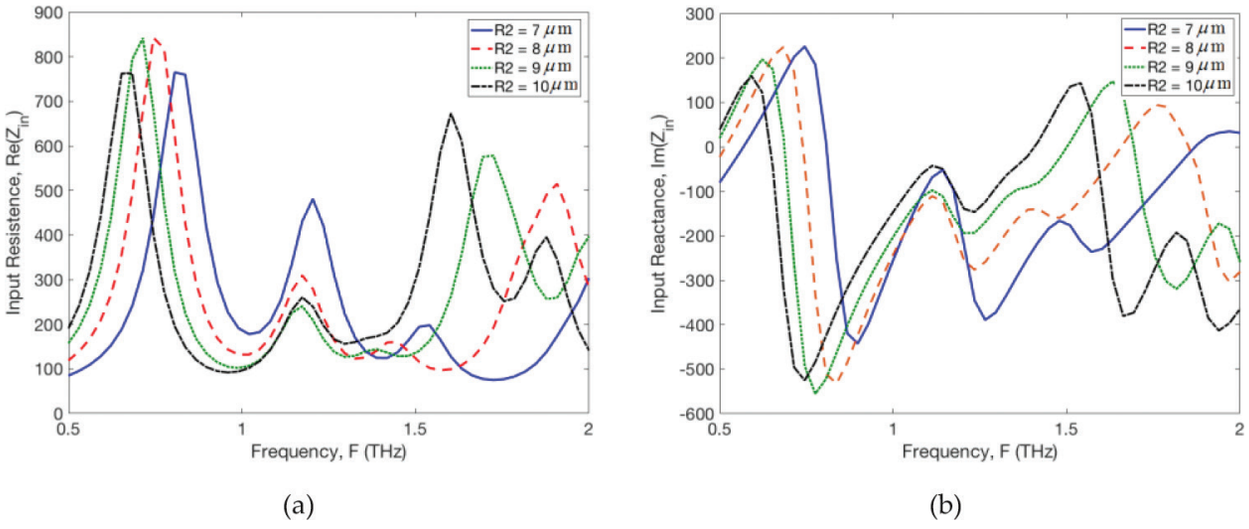

(a) (b)

Figure 8. Input impedance for antennas with H = 1 μm, where R1 = 0.4 × R2, R2 = 7, 8, 9, and 10 μm: (a) input resistance (Re(Z_{in})) and (b) input reactance (Im(Z_{in})).

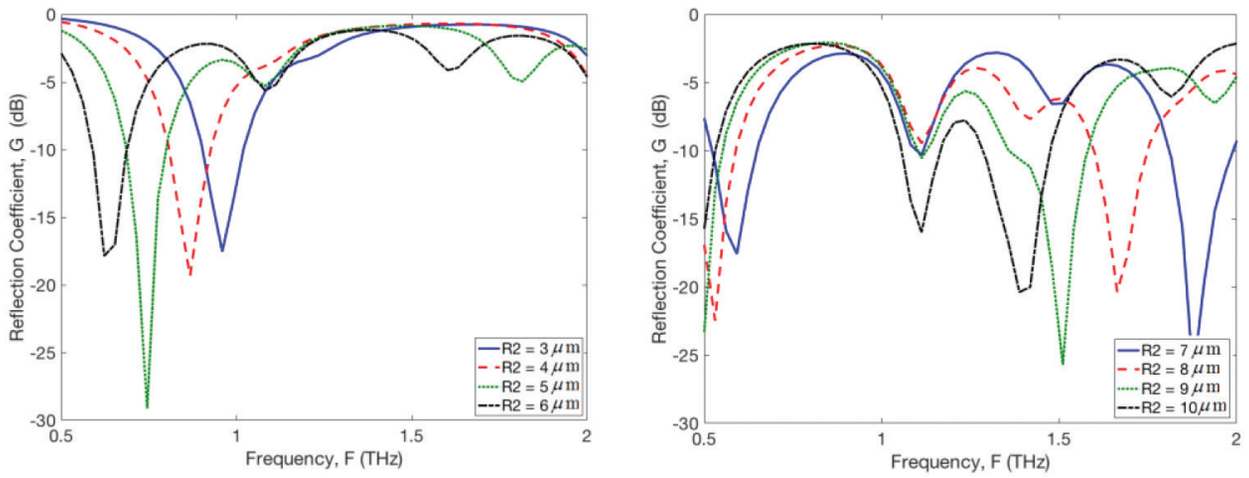

(a) (b)

Figure 9. Reflection coefficient of antennas of **Figures 6** and **7**. (a) R2 = 3, 4, 5, and 6 μm (Z_c = 80 Ω). (b) R2 = 7, 8, 9, and 10 μm (Z_c = 150).

To compare the bandwidth of these antennas, we calculated the fractional bandwidth defined by $B(\%) = 200 \times (f_H - f_L)/(f_H + f_L)$, where f_H and f_L are the superior and inferior, respectively, limits of the band for a level of −10 dB. The results are presented in **Table 3**, where the fractional bandwidth for all simulations for the case H = 1 mm is presented. We observe that the best case is R2 = 7 mm with R1 = 0.4 × R2, where B = 21.7%.

For the case with broad bandwidth of **Table 3** (R1 = 0.4 × R2 and R2 = 7 μm), we plot the normalized radiation diagram at F = 0.56 THz in the middle of the bandwidth in **Figure 10**. The diagram is an asymmetric version of that diagram of an isolated dipole. The asymmetry is due to the asymmetric geometry of the antenna in the xz plane. This diagram radiates more energy in the –z direction, where in this case, the loop acts as a reflector element.

http://dx.doi.org/10.5772/intechopen.74936

Fractional bandwidth, *B*(%)			
	R1		
R2	0.4 × R2	0.6 × R2	0.8 × R2
3 μm	12.1	14.7	11.2
4 μm	13.7	10.7	10.7
5 μm	15.4	6.9	10.1
6 μm	15.4	4.6	10.2
7 μm	21.7	11.7	15.3
8 μm	9.0	12.6	14.4
9 μm	2.2	18.7	14.5
10 μm	9.9	17.7	14.6

Table 3. Fractional bandwidth of dipole-loop antennas with H = 1 μm.

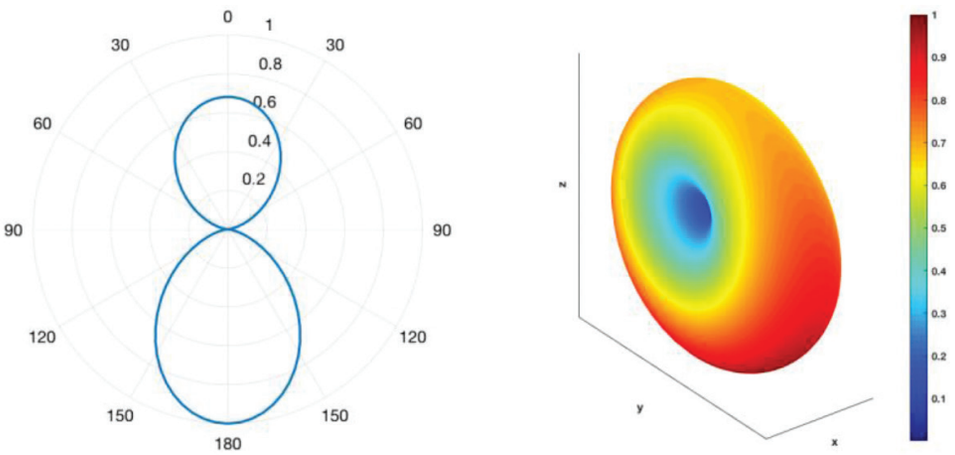

(a) (b)

Figure 10. Normalized radiation diagram of antennas with a higher bandwidth (R2 = 7 μm, R1 = 0.4 × R2) at F = 56THz, in the middle of the bandwidth. (a) 2D diagram at plane *xz*. (b) 3D diagram.

4.2.2. Effect of chemical potential

In this section, we present the variation of the characteristic of the antennas as a function of the chemical potential of the loop. The dimensions of the loop and the dipole were fixed as $W = 17\ \mu$m, $L = 10\ \mu$m, $H = 1\ \mu$m, R2 = 5 μm, and R1 = 0.4 × R2. The chemical potential of the dipole is $\mu_C = 0.13$ eV and the loop is varied $\mu_C = 0$, 0.03, 0.07, 0.1 and 0.13 eV. **Figure 11** shows the geometry and MoM mesh for this antenna.

Figures 12 and **13** show the input impedance and reflection coefficient obtained, respectively. In **Figure 13**, we used $Z_c = 300\ \Omega$, for $\mu_C = 0$, 0.07, 0.1, and 0.13 eV, and for $\mu_C = 0.03$ eV, we used $Z_c = 150\ \Omega$. These values of the Zc produce a better bandwidth.

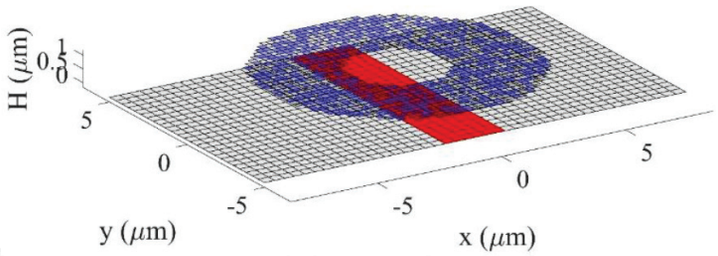

Figure 11. Geometry and MoM mesh of dipole-loop antenna with 17 μm, $L = 10$ μm, $H = 1$ μm, R2 = 5 μm, and R1 = 0.4 × R2.

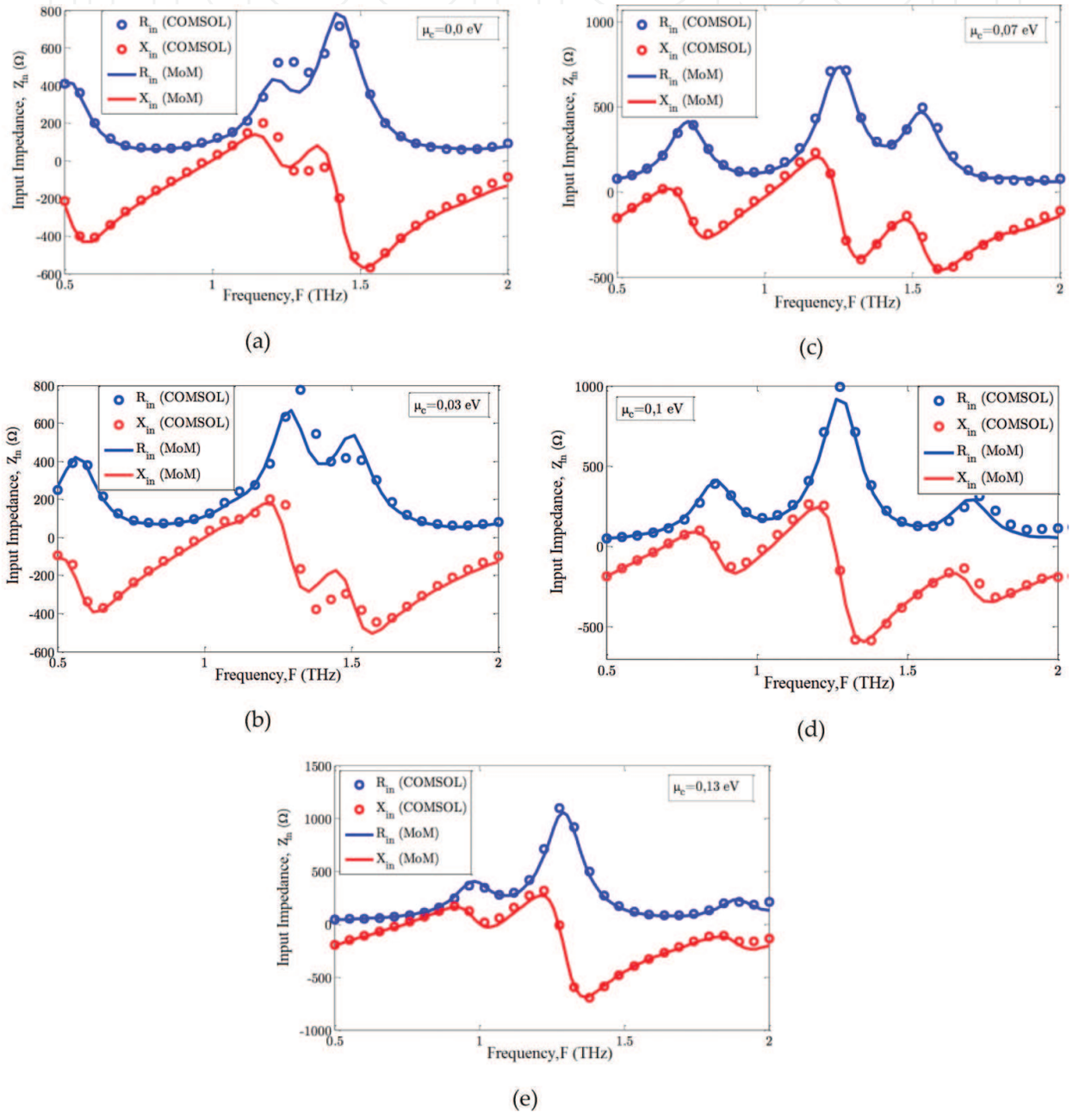

Figure 12. Input impedance variation with the chemical potential of loop. Geometry of dipole-loop antenna is $W = 17$ μm, $L = 10$ μm, $H = 1$ μm, R2 = 5 μm, and R1 = 0.4 × R2 ($\mu_C = 0.13$ eV for dipole). Chemical potential of loop are: (a) $\mu_C = 0.0$ eV; (b) $\mu_C = 0.03$ eV; (c) $\mu_C = 0.07$ eV; (d) $\mu_C = 0.1$ eV; and (e) $\mu_C = 0.13$ eV.

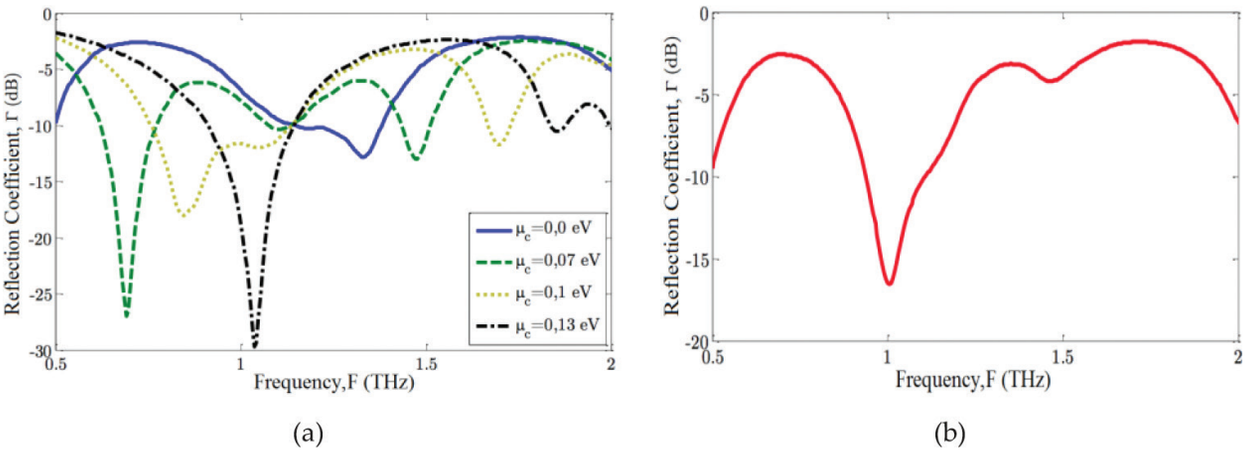

Figure 13. Variation of reflection coefficient with loop's chemical potential. Data of dipole-loop antenna: W = 17 μm, L = 10 μm, H = 1 μm, R2 = 5 μm, and R1 = 0.4 × R2 (μ_C = 0.13 eV for dipole), chemical potential of loop (a) μ_C = 0.0, 0.07, 0.1, and 0.13 eV (Z_c = 300 Ω), and (b) μ_C = 0.03 eV (Z_c = 150 Ω).

Fractional bandwidth *B*(%)					
μ_C (eV)	0.0	0.03	0.07	0.1	0.13
B (%)	22.4	16.9	21.5	43.5	26.8

Table 4. Fractional bandwidth for the antennas of **Figure 13**.

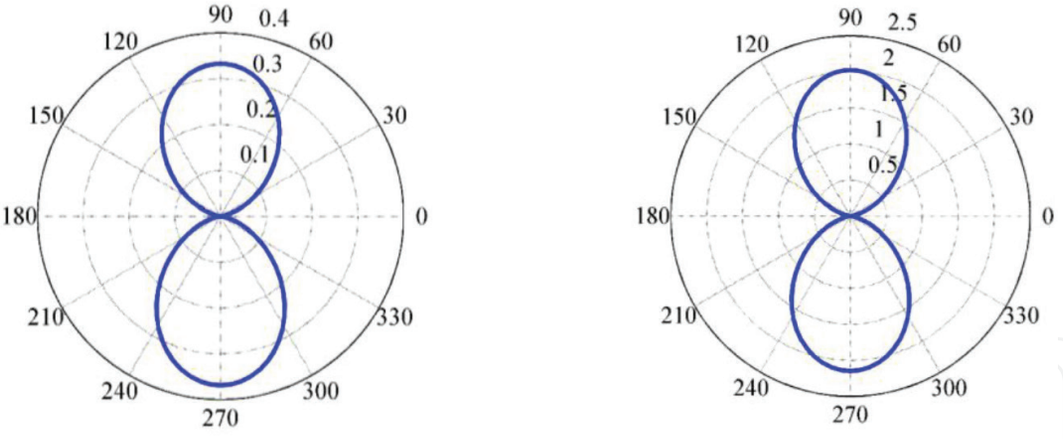

Figure 14. 2D radiation diagram of gain at plane xy and in frequencies (a) F = 0.69 THz (first resonance) and (b) F = 0.85 THz (second resonance). Data of antenna: W = 17 μm, L = 10 μm, H = 1 μm, R2 = 5 μm, and R1 = 0.4 × R2, μ_C = 0.13 eV (for dipole) μ_C = 0.1 eV (for loop).

First, we observe a better agreement between MoM and Comsol. Also, we note that we can control the effect of the loop in the total input impedance by varying its chemical potential.

We observe in **Figure 12** that only the resonance of loop is modified with chemical potential. For example, in **Figure 12c**, the loop resonance is near F = 0.75 THz, and in **Figure 12d**, it is near F = 0.8 THz.

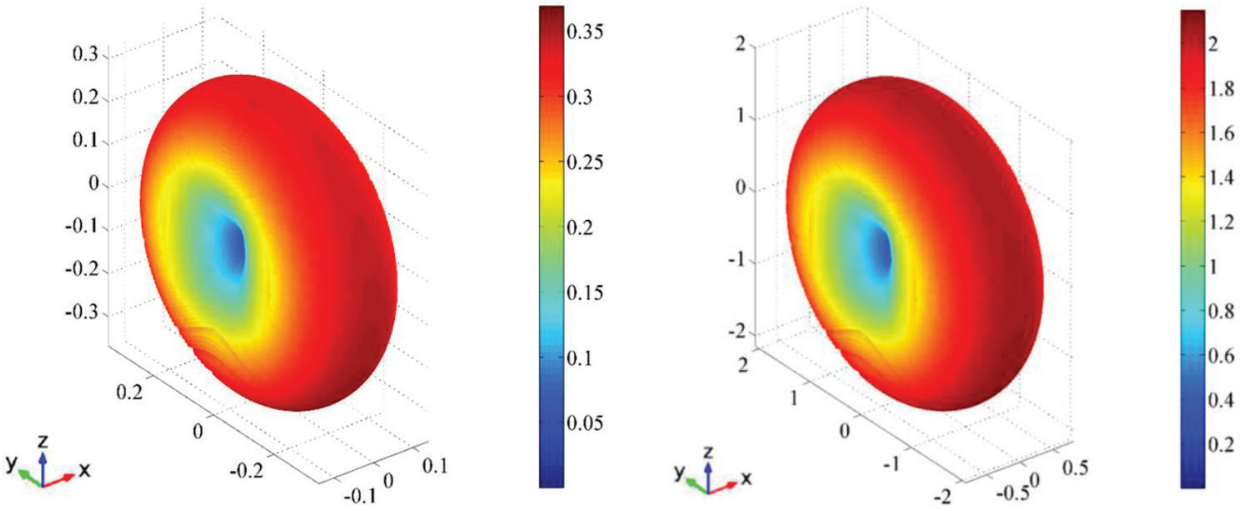

(a) (b)

Figure 15. 3D radiation diagram of gain at frequencies (a) F = 0.69 THz (first resonance) and (b) F = 0.85 THz (second resonance). Data of antenna: W = 17 μm, L = 10 μm, H = 1 μm, R2 = 5 μm, and R1 = 0.4 × R2, μ_C = 0.13 eV (for dipole) μ_C = 0.1 eV (for loop).

The results of **Figure 13** were obtained for Z_c = 300 Ω; however for the case of μ_C = 0.03 eV, we used Z_c = 150 Ω. These values of Z_c presented a better bandwidth. The bandwidth obtained are presented in **Table 4**, where the broad bandwidth was found for the case with μ_C = 0.7 eV.

The resonant frequencies for the best bandwidth (μ_C = 0.1 eV) are F = 0.69 and 0.85 THz, as can be seen in **Figure 12d**, where the reactance is null. The radiation diagrams in these frequencies are presented in **Figures 14** and **15**. We observe that these diagrams are more symmetrical and similar to that of isolated dipole. This is because the size of the loop element is smaller than that of **Figure 10**; therefore, the effect of their surface current to produce far field is smaller.

5. Conclusions

In this book chapter, we presented a numerical analysis of a broadband graphene dipole-loop antenna for terahertz application. In this antenna, only the dipole element is fed by a voltage source, while the loop element is electromagnetically coupled to the dipole. The bidimensional method of moment, with an equivalent surface impedance of graphene, was used for numerical calculations, and some results are obtained by finite element method for comparison. A good agreement between these two methods was obtained, but the method of moment is faster than the finite element method. In the results, we first presented a review of the principal characteristics of the conventional graphene dipole antenna. Then, we analyzed the broadband characteristics of the graphene dipole-loop antenna as a function of geometry and chemical potential of the loop. The results show that these parameters can be used to enhance the fractional bandwidth of this antenna, where a combination of these two parameters in the optimization process produces better results than one alone. The best antenna obtained presented a fractional bandwidth of 43.5% with a radiation diagram with linear polarization and good symmetry properties.

Acknowledgements

The authors would like to thank the Mr. Mauro Roberto Collatto Junior Chief Executive Officer of the Junto Telecom Company for the financial and emotional support to this project.

Conflict of interest

The authors declare that there is no conflict of interest regarding the publication of this work.

Author details

Karlo Queiroz da Costa[1]*, Gleida Tayanna Conde de Sousa[2], Gabriel Silva Pinto[2] and Andrey Viana Pires[2]

*Address all correspondence to: karlo@ufpa.br

1 Department of Electrical Engineering, Federal University of Para, Tucuruí-PA, Brazil

2 Department of Electrical Engineering, Federal University of Para, Belém-PA, Brazil

References

[1] Akyildiz IF, Jornet JM, Han C. Terahertz band: Next frontier for wireless communications. Physics Communications. 2014;**12**:16-32

[2] Koch M. Terahertz communications: A 2020 vision. In: Miles R, Zhang XC, Eisele H, Krotkus A, editors. Terahertz Frequency Detection and Identification of Materials and Objects, NATO Security through Science Series. Vol. 19. Springer; 2007. pp. 325-338

[3] Piesiewicz R, Kleine-Ostmann T, Krumbholz N, Mittleman D, Koch M, Schoebel J, Kurner T. Short-range ultra-broadband terahertz communications: Concepts and perspectives. IEEE Antennas and Propagation Magazine. 2007;**49**(6):24-39

[4] Federici J, Moeller L. Review of terahertz and subterahertz wireless communications. Journal of Applied Physics. 2010;**107**(11):111101

[5] Huang K-C, Wang Z. Terahertz terabit wireless communication. IEEE Microwave Magazine. 2011;**12**(4):108-116

[6] Kleine-Ostmann T, Nagatsuma T. A review on terahertz communications research. Journal of Infrared, Millimeter and Terahertz Waves. 2011;**32**:143-171

[7] Song H, Nagatsuma T. Present and future of terahertz communications. IEEE Transactions on Terahertz Science and Technology. 2011;**1**(1):256-263

[8] Kürner T, Priebe S. Towards THz communications-status in research, standardization and regulation. Journal of Infrared, Millimeter and Terahertz Waves. 2014;**35**(1):53-62

[9] Geim A, Novoselov K. The rise of graphene. Nature Materials. March 2007;**6**(3):183-191

[10] Fang Z et al. Graphene-antenna sandwich photodetector. Nano Letters. June, 2012: 3808-3813

[11] Schwierz F. Graphene transistors. Nature Nanotechnology. May 2010

[12] Perruisseau-Carrier J. Graphene for antenna applications–Opportunities and challenges from microwaves to THz. Loughborough Antennas & Propagation Conference, UK. 2012

[13] Tamagnone M, Gómez-Díaz JS, Mosig JR, Perruisseau-Carrier J. Analysis and design of terahertz antennas based on plasmonic resonant graphene sheets. Journal of Applied Physics. December 2012;**112**

[14] Zhang H, Jiang Y, Wang J. A broadband terahertz antenna using graphene. 11th International Symposium on Antennas, Propagation and EM Theory (ISAPE), Antennas, Propagation and EM Theory (ISAPE), Guilin, China. 18-21 October 2016

[15] da Costa KQ, Dimitriev V, Nascimento CM, Silvano GL. Theoretical analysis of graphene nanoantennas with different shapes. Microwave and Optical Technology Letters. May 2014;**56**(5)

[16] da Costa KQ, Dimitriev V. Planar monopole UWB antennas with cuts at the edges and parasitic loops. InTech: Ultra Wideband Communications: Novel Trends—Antennas and Propagation, 1st ed., pp. 143-145, 2011

[17] COMSOL Multiphysic 4.4, COMSOL Inc., http://www.comsol.com

[18] Hanson GW. Dyadic Green's functions and guided surface waves for a surface conductivity model of Graphene. Journal of Applied Physics. 2008;**103**:064302